The impact of continental width on tropical precipitation

Elizabeth A. Maroon[1] and Dargan M. W. Frierson[1]

Corresponding author: Elizabeth Maroon, Department of Atmospheric Sciences, University of Washington, Seattle, WA, USA. (emaroon@atmos.washington.edu)

[1]Department of Atmospheric Sciences,

University of Washington, Seattle,

Washington, USA.

Key Points.

- Decreased evaporation is important in setting precipitation change from the addition of a continent
- In a more comprehensive model, radiative feedbacks dominate the interhemispheric energy budget
- Balance between the area of low clouds and continent sets the location of greater precipitation

The location of continents affects tropical precipitation in a variety of ways. Here, we examine how the longitudinal extent of a Northern Hemisphere (NH) subtropical continent impacts the distribution of tropical precipitation in two otherwise aquaplanet general circulation models of varying complexity. Dark continents are first studied with albedo set equal to the surrounding ocean. Then higher, more realistic continental albedo values are used.

In the first simpler model, the addition of land decreases evaporation and precipitation in the NH, which scales with the width of the continent. In the second comprehensive model,

precipitation and circulation changes have zonal variation due to cloud and water vapor feedbacks. As the continent widens in this model, more precipitation shifts towards the continent. In both models, a brighter albedo shifts precipitation southward. The difference in precipitation responses between the two models points to the importance of radiative feedbacks in enhancing circulation shifts.

1. Introduction

Tropical precipitation falls where there is large scale ascent: in the monsoon regions and in the Intertropical Convergence Zone (ITCZ). As such, the dynamics of monsoon and Hadley circulations are key to understanding precipitation. However, it is hard to disentangle these two circulations: for example, during the solsticial seasons, the bulk of the Hadley circulation occurs in the region of the Asian monsoon [*Dima and Wallace*, 2003]. Many studies have considered the monsoon in frameworks developed for the Hadley circulation [*Chao and Chen*, 2001; *Gadgil*, 2003; *Privé and Plumb*, 2007; *Bordoni and Schneider*, 2008; *Merlis et al.*, 2013a], rather than through land-sea contrast [*Webster*, 1987]. As such, monsoon precipitation can be thought of as a seasonal displacement of the ITCZ over land.

There are two strong constraints on the zonal mean tropical circulation: an angular momentum constraint [*Held and Hou*, 1980; *Lindzen and Hou*, 1988; *Plumb and Hou*, 1992; *Bordoni and Schneider*, 2008] and an energetic constraint [*Broccoli et al.*, 2006; *Kang et al.*, 2008, 2009; *Donohoe et al.*, 2013; *Schneider et al.*, 2014]. Angular momentum is nearly conserved when the Rossby number is large during the solstice seasons, but does not provide a constraint on the circulation strength [*Bordoni and Schneider*, 2008; *Merlis et al.*, 2013b]. The energetic constraint, when applicable (see *Kang et al.* [2009]; *Merlis et al.* [2013b]; *Shaw et al.* [2015]), does provide information on circulation strength and the ITCZ location. Energy is transported from one hemisphere to the other by the upper branch of the Hadley circulation; by mass conservation, the lower branch transports moisture in the opposite direction. Because temperatures are constrained in the tropical free troposphere

[*Sobel et al.*, 2001], temperature anomalies at the edge of the subtropics (which is related to midlatitude energy transport by eddies) can affect energy transport and circulation through the whole Hadley circulation regime. This relation between interhemispheric temperature gradients and tropical precipitation can help us understand shifts in tropical precipitation in the recent and deeper past [*Chiang and Bitz*, 2005; *Broccoli et al.*, 2006; *Frierson and Hwang*, 2012; *Hwang et al.*, 2013].

We focus on the energetic perspective and examine how the presence of land affects tropical precipitation. We build upon *Maroon et al.* [in revision], which examines the addition of a single continent in aquaplanet models and found that precipitation shifted southward as the albedo of the continent was increased. In the more complex of the two models (AM2.1), the tropical precipitation response had azonal structure due to the formation of low clouds to the west of the continent. These low clouds had a strong SW cloud radiative effect that cooled the NH relative to the SH; this feedback reinforced the albedo forcing which tended to shift precipitation southward. This result led us to another question: what if the continent's width spanned far enough to change the near-balance between the stratus cloud feedbacks and cloud feedbacks in other regions? Here we test how continent width affects the distribution of tropical precipitation and the net top-of-atmosphere (TOA) radiation. Our configuration is similar to that in *Merlis et al.* [2013a], but the addition of radiative feedbacks and varying land geometries provides an interesting contrast between the two studies.

2. Models

We configure two GCMs of differing complexities as aquaplanets with simple continents. The first model is the gray radiation model (GRaM), which includes the effect of latent heating by moisture, but does not include clouds or the radiative effect of water vapor [*Frierson et al.*, 2006]. The second model is the finite volume numerics GFDL AM2.1 which has comprehensive parameterizations of atmospheric physics [*Anderson et al.*, 2004]; the exact code used was first configured by [*Shi and Durran*, 2014]. Annual mean insolation is used in both models; simulations with a seasonal cycle are described in *Maroon et al.* [in revision].

An aquaplanet simulation is used as the control for both models, and additional simulations add idealized subtropical continents that vary in width. In the AM2.1 control, the width of the ITCZ is very narrow, and as a result, any precipitation changes in this model will be larger than in the GRaM. All continents span from 10°N to 30°N. Two continental simulations were conducted with GRaM: one with a 60° wide continent and one with a 360° wide continent. AM2.1 simulations with continent widths of 60°, 120°, 180°, 240°, 300°, and 360° are shown. The albedo of all continents is the same as that of the ocean in the subtropics; thus, the interhemispheric difference in net radiation due to surface albedo is near-zero. Because GRaM does not have clouds, the ocean albedo is set to 0.29 to produce more realistic energy budgets. In AM2.1, the ocean albedo is approximately 0.06 in the subtropics. Both models use similar versions of LM2 [*Milly and Shmakin*, 2002], but with differing land parameters. See *Maroon et al.* [in revision]; *Scheff*

[2014] for a description of the model and these parameters. Both models are spun up for 5 years, with an additional 5 years used for climatology.

3. Results

3.1. GRaM simulation results

In both 60° and 360° dark-continent GRaM simulations, precipitation decreases over the continent, in the NH deep tropics south of the continent, and immediately north of the continent (Figure 1a, blue lines). The time and zonal-mean moisture budget states that changes in precipitation (P) are balanced by changes in evaporation (E) and moisture flux convergence. As shown in *Kang et al.* [2009], changes in the cross-equatorial moisture transport are proportional to changes in cross-equatorial energy transport, if changes in evaporation and gross moist stability are small. If changes in evaporation are not small, then there is a relation between changes in P-E (rather than P alone) and the cross-equatorial heat transport.

In these simulations, the changes in tropical precipitation are dominated by changes in evaporation (Figure 1a, red lines). Evaporation has decreased because an unsaturated land surface replaced a previously wet surface. The surface temperature has also increased, due to the lower tropospheric moisture decrease promoting a dry adiabatic lapse rate, while upper-level temperatures remains the same. The increased heating of the continent drives lower-tropospheric convergence (Figure 1c) at the southern edge of the continent. This drives moist surface air toward the continent and away from the ITCZ, decreasing equatorial precipitation. Over the continent, the increased moisture convergence feeds an additional decrease in evaporation.

These precipitation changes occur only in the longitude bands that are occupied by the continent. Elsewhere, precipitation and evaporation change minimally. Figure 1a&b shows the 60° simulation precipitation and evaporation (light blue and red lines) multiplied by a factor of six to directly compare with the 360° wide simulation. Because the hydrologic changes are zonally confined to the continental region in the 60° wide simulation, the response of precipitation is proportional to continent width.

When the albedo is increased in the light continent simulations, there is a small increase in precipitation in the SH. Precipitation has shifted slightly southward across the equator in response to the interhemispheric difference in net heating. The change in precipitation is nearly linear with continent width in these light simulations as well. Figure 1b shows that the precipitation and evaporation responses between the 360° wide light simulation and six times the 60° wide light simulation are nearly the same.

NH-SH precipitation, NH-SH evaporation, and the cross-equatorial energy transport measure the hemispheric asymmetry of precipitation and which processes promote it; Figure 2 shows these quantities for all the simulations and summarizes the changes in each simulation. For both dark continents in GRaM, the change in NH-SH evaporation almost completely balances the change in NH-SH precipitation (the bright red markers in Figure 2a). The change in energy transport across the equator is not responsible for the precipitation changes. In Figure 2b, the 360° dark simulation (red square) has increased northward energy transport and northward shifted precipitation when compared to the 60° continent (red circle). If anomalous Hadley circulation transport changes were responsible for $P - E$ changes, you would expect these two quantities to be oppositely

related. Instead, the land-induced circulation change in this simulation is shallow (Figure 1c), which changes the gross moist stability. With a minimum in moist static energy in the mid-troposphere, there is negative gross moist stability in the bottom-heavy circulation [*Back and Bretherton*, 2006]. This reverses the relation between energy transport and $P - E$ that will be seen later with the AM2.1 simulations that have deep circulation changes.

In the light continent simulations where there is a more visible shift, NH-SH evaporation balances approximately 90% of the change in NH-SH precipitation (light red markers in Figure 2). After accounting for evaporation, only 10% of the precipitation change can be attributed to a change in cross-equatorial energy transport.

3.2. AM2.1 simulation results

In the AM2.1 simulations with dark continents of varying width, there are also noticeable hemispheric changes in both precipitation and evaporation in the deep tropics and NH subtropics (Figure 1d&e, and dark blue markers in Figure 2a). As mentioned above, shifts in precipitation are larger than in their GRaM counterparts because of the sharper ITCZ in AM2.1. Regardless of continent width, evaporation decreases over the continent about the same absolute amount as in the GRaM simulations, again because of decreased surface water availability. The higher land surface temperature in AM2.1 also induced surface convergence at the edge of the southern continent, again like the GRaM simulations (Figure 1f).

However, in contrast to the GRaM simulations, the location of greater precipitation changes with continent width. As the continent width increases, precipitation shifts more

into the NH (Figure 2 and Figure 3). In these dark simulations, the changes in evaporation do not explain the changes in precipitation, which are much larger and oppose the evaporation changes (Figure 2a). NH evaporation decreases, while NH precipitation increases. The change in heat transport across the equator balances the change in the NH-SH $P - E$ (Figure 2b). A deep anomalous Hadley circulation transports heat from NH to SH and moisture from SH to NH, countering the decrease in evaporation. The larger the change in energy transport across the equator, the larger the change in zonal $P - E$.

For the narrower continents, the change in the zonal structure of precipitation is composed of opposing regional changes in precipitation (shading in Figure 3). To the west of the continent, low stratus clouds form which cool the SST in the NH and shift precipitation in this region southward. This effect decreases slightly as the continent widens, but the bulk of the SW cloud radiative effect (CRE) from these low clouds largely remains until the 360° continent paves over the whole NH subtropical ocean (shading in Figure 4).

In the continental region, precipitation shifts toward the hot continent and decreases along the equator in association with an anomalous overturning cell that has its ascending branch at the southern edge of the continent (Figure 1f). To the east of the continent, precipitation also shifts slightly into the NH. As the continent widens, more precipitation shifts toward the continent relative to the southward stratus-related shift, which decreases slightly in extent with continent width. As a result, the wider the continent is, the more precipitation there is in the NH. The northward precipitation shift in this zone is proportional with the width of the continent (Figure 1d and Figure 3). The wider the

continent, the wider the ascending region. We can understand the zonal precipitation shift as the sum of a southward shift in the stratus region and a northward shift that increases with continent width. Both regional shifts act to move precipitation away from the equator in the zonal mean (Figure 1d).

As more precipitation shifts toward the continent, deep clouds and greater moisture also shift into the NH. As a result, where precipitation increases, there is also an increase in NH energy content due to decreased outgoing net radiation (Figure 3). In the dark AM2.1 continent simulations, the combined longwave (LW) CRE and LW clear-sky radiation (which both increase energy in the hemisphere with precipitation) are greater than the shortwave (SW) CRE (which acts to decrease energy in the hemisphere with precipitation). Having greater TOA net LW than SW results in greater absorbed energy in the NH than SH (contours and shading in Figure 4). Given the complexity of cloud parameterizations, other GCMs could have a different balance between TOA LW and SW. The changes in net TOA radiation in the SH are small in comparison to the NH changes in the continental region. Because the change in TOA net radiation from clouds and water vapor acts to increase the cross-equatorial energy transport, these cloud and clear-sky effects are a positive interhemispheric feedback that further increases the interhemispheric asymmetry of precipitation and the anomalous Hadley circulation.

The increase in NH precipitation with continent width can be understood through the sum of regional changes; the amount of net radiation in the NH continental region increases with continent width, while the reflected SW in the stratus cloud region stays the same size. Aw a result, there is a relation between continent width and $P - E$ (triangles in

Figure 2b). Aside from the surface change from the dark continent, there is no other forced asymmetry between the hemispheres. The cloud and water vapor feedbacks amplify the large changes in zonal precipitation.

When the albedo of the 60° and 360° wide continents is increased to 0.20 and 0.30, the northward precipitation shift decreases (light blue and green markers in Figure 2). The higher NH surface albedo creates an interhemispheric asymmetry in net TOA radiation between the hemispheres that shifts precipitation southward relative to the dark continent. When the 360° wide AM2.1 continent has an albedo of 0.20, there is almost no interhemispheric precipitation asymmetry: the surface albedo has NH-SH net TOA radiation that is countered by the oppositely-signed NH-SH net TOA radiation from the cloud and water-vapor feedbacks from the land-induced circulation. The cloud and clear sky feedbacks in the continental region are key for setting the overall zonal response. With a continental albedo of 0.30, in both the 60° and 360° continents, zonal mean precipitation shifts into the SH. Once albedo is high, the change in NH-SH precipitation is roughly the same for the 60° and 360° wide continents and additional energy transport has little effect (green markers in Figure 2); instead, additional changes in E now balance changes in P.

4. Discussion

We have shown that the response of tropical precipitation to a simple idealized continent can vary greatly depending on the characteristics of that continent and the specifics of the GCM used. Without cloud or water vapor radiative feedbacks, the change in tropical precipitation location in GRaM simulations is almost completely due to changes in evaporation over the added land surface. Regardless of continent width, the change in

precipitation is local to the band where land is added. Precipitation decreases in the NH, and displays a small southward shifts if the albedo of continent is higher than that of the ocean.

In AM2.1 simulations, there are larger changes in precipitation, evaporation, and circulation. The NH-SH precipitation asymmetry is composed of a precipitation shift toward the continent and a precipitation shift away from the stratus deck that forms downstream of the continent. As the continent widens, the precipitation that is drawn toward the continent in a monsoon-like flow also widens, and becomes relatively larger than the southward precipitation shift in the stratus region. Changes in LW CRE, SW CRE, and clear sky radiation accompany the precipitation shift. The net TOA LW outweighs the SW CRE from the deep convective clouds and the stratus deck. With no initial land-ocean albedo difference, these changes in net radiation due to the cloud and clear sky feedbacks are responsible for amplifying the northward shift zonal mean precipitation. Increasing albedo shifts precipitation away from the hemisphere with the continent, modulating the effect of continental width.

If we compare the change from aquaplanet in GRaM and AM2 in the dark-albedo 360° simulations, the precipitation responses in the models are quite different from each other though both have anomalous ascent at the continent's southern edge. In GRaM, precipitation decreased in the continent's hemisphere, while in AM2.1, precipitation shifted to the continent. While in GRaM, this precipitation change is attributed to evaporation, energy transport across the equator in GRaM is northward, while it is also southward in its AM2.1 counterpart. In GRaM, energy transport at the equator is northward due to

greater OLR over the hot continent. In AM2.1, energy transport is southward due to the combination of positive LW CRE and decreased clear-sky OLR that outweighs the negative SW CRE in the tropical and subtropical NH. Although there are other differences between the two models, the difference in the direction of cross-equatorial energy transport is likely due to the presence of cloud and water vapor feedbacks in AM2.1. When the continent heats up in AM2.1, it does not radiate the energy to space as GRaM's continent does; the feedbacks invert the energy transport response at the equator from what would be expected in their absence. As recently shown by *Shaw et al.* [2015], feedbacks can play unexpectedly important roles in the zonal rectification of equatorial energy transport and precipitation shifts.

These simulations are idealized, but they support the suggestion in *Frierson et al.* [2013] that the role of the Sahara in isolation would be to decrease NH energy content and shift zonal mean precipitation southward. It also points to the importance of interhemispheric radiative feedbacks on the land circulation. With uncertainty in the relative SW and LW responses of clouds across models, whether a land-induced anomalous zonal circulation is enhanced or damped by the cloud response could vary in other models.

Acknowledgments. E.A.M. was supported by an NDSEG fellowship and IGERT Program on Ocean Change traineeship. D.M.W.F was supported by NSF grants AGS-1359464 and PLR-1341497, and a UW Royalty Research Fund grant. We thank Jacob Scheff for assistance with the AM2.1 model setup. Model output from this study is available at http://atmos.washington.edu/ emaroon/continentwideningoutput

References

Anderson and Coauthors (2004), The new GFDL global atmosphere and land model AM2599 LM2: Evaluation with prescribed SST simulations, *J. Climate*, *17*, 4641–4673.

Back, L. E. and C. S. Bretherton (2006), Geographic variability in the export of moist static energy and vertical motion profiles in the tropical Pacific, *Geophys. Res. Lett.*, *33*, L17810, doi:10.1029/2006GL026672.

Bordoni, S. and T. Schneider (2008), Monsoons as eddy-mediated regime transitions of the tropical overturning circulation, *Nature Geosci.*, *1*, 515–519.

Broccoli, A. J., K. A. Dahl, and R. J. Stouffer (2006), Response of the ITCZ to northern hemisphere cooling, *Geophys. Res. Lett.*, *33*, L01702.

Chao, W. C. and B. Chen (2001), The origin of monsoons, *J. Atmos. Sci.*, *58*(22), 3497–3507.

Chiang, J. C. H. and C. M. Bitz (2005), Influence of high latitude ice cover on the marine Intertropical Convergence Zone, *Clim. Dyn.*, *25*, 477–496.

Dima, I. M. and J. M. Wallace (2003), On the seasonality of the Hadley Cell, *J. Atmos. Sci.*, *60*, 1522-1527.

Donohoe, A., J. Marshall, D. Ferreira, and D. McGee (2013), The relationship between ITCZ location and cross-equatorial atmospheric heat transport: from the seasonal cycle to the last glacial maximum, *J. Climate*, *26*, 3597–3618.

Frierson, D. M. W., I. M. Held, and P. Zurita-Gotor (2006), A gray radiation aquaplanet moist GCM. Part I: Static stability and eddy scale, *J. Atmos. Sci 63*, 2548–2566.

Frierson, D. M. W. and Y.-T. Hwang (2012), Extratropical influence on ITCZ shifts in slab ocean simulations of global warming, *J. Climate 25*, 720–733.

Frierson, D. M. W., Y.-T. Hwang, N. S. Fučkar, R. Seager, S. M. Kang, A. Donohoe, E. A. Maroon, X. Liu and D. S. Battisti (2013), Contribution of ocean overturning circulation to 647 tropical rainfall peak in the Northern Hemisphere, *Nature Geosci.*, *49*(14), 1233–1241.

Gadgil, S. (2003), The Indian monsoon and its variability, *Annu. Rev. Earth Planet. Sci.*, *31*, 429–467.

Held, I. M. and A. Y. Hou (1980), Nonlinear Axially Symmetric Circulations in a Nearly Inviscid Atmosphere, *J. Atmos. Sci.*, *37*(3), 515–533.

Hwang, Y.-T., D. M. W. Frierson, and S. M. Kang (2013), Anthropogenic sulfate aerosol and the southward shift of tropical precipitation in the 20th century, *Geophys. Res. Lett* *40*, 1–6.

Kang, S. M., I. M. Held, D. M. W. Frierson, and M. Zhao (2008), The response of the ITCZ to extratropical thermal forcing: Idealized slab-ocean experiments with a GCM, *J. Climate*, *21*(14), 3521–3532.

Kang, S. M., D. M. W. Frierson, and I. M. Held (2009), The tropical response to extratropical thermal forcing in an idealized GCM: the importance of radiative feedbacks and convective parameterization, *J. Atmos. Sci.*, *66*(9), 2812–2827.

Lindzen, R. S. and A. Y. Hou (1988), Hadley circulations for zonally averaged heating centered off the equator, *J. Atmos. Sci.*, *45*, 2416–2427.

Maroon, E. A., D. M. W. Frierson, S. M. Kang and J. Scheff (in revision), The precipitation response to an idealized subtropical continent.

Merlis, T. M., T. Schneider, S. Bordoni, and I. Eisenman (2013), Hadley circulation response to orbital precession. Part I: Aquaplanets, *J. Climate*, *26*, 740–753.

Merlis, T. M., T. Schneider, S. Bordoni, and I. Eisenman (2013), Hadley circulation response to orbital precession. Part II: Subtropical Continent, *J. Climate*, *26*, 754–771.

Milly P. C. D. and A. B. Shmakin (2002), Global Modeling of Land Water and Energy Balances. Part I: The Land Dynamics (LaD) Model, *J. Hydrometeor.*, *3*, 283–299.

Plumb, R. A. and A. Y. Hou (1992), The response of a zonally symmetric atmosphere to subtropical thermal forcing: Threshold behavior. *J. Atmos. Sci.*, *49*, 1790–1799.

Privé, N. C. and R. A. Plumb (2007), Monsoon dynamics with interactive forcing. Part I: Axisymmetric studies, *J. Atmos. Sci.*, *64*, 915–934.

Scheff, J. (2014), Understanding the responses of precipitation, evaporative demand, and terrestrial water availability to planetary temperature in climate models. PhD Dissertation, Department of Atmospheric Sciences, University of Washington, 199pp, http://www.ldeo.columbia.edu/ jscheff/JacobScheffUWDissertation.pdf

Schneider, T., T. Bischoff, and G. H. Haug (2014), Migrations and dynamics of the intertropical convergence zone, *Nature*, *513*, 45–53.

Shaw, T. A., A. Voigt, S. M. Kang and J. Seo (2015), Response of the intertropical convergence zone to zonally-asymmetric subtropica surface forcings, *Geophys. Res. Lett.*, *42*, doi:10.1002/2015GL066027.

Shi, X. and D. R. Durran (1992), The Response of Orographic Precipitation over Idealized Mid-Latitude Mountains Due to Global Increases in CO2, *J. Climate*, *27*, 3938–3956.

Sobel, A. H., J. Nilsson, and L. M. Polvani (2001), The Weak Temperature Gradient Approximation and Balanced Tropical Moisture Waves, *J. Atmos. Sci.*, *58*, 3650–3665.

Webster, P. J. 1987 *The elementary monsoon.* In Fein, J. S. and Stephens, P. L. (eds.) Monsoons, 3-32 (John Wiley & Sons, New York, NY)

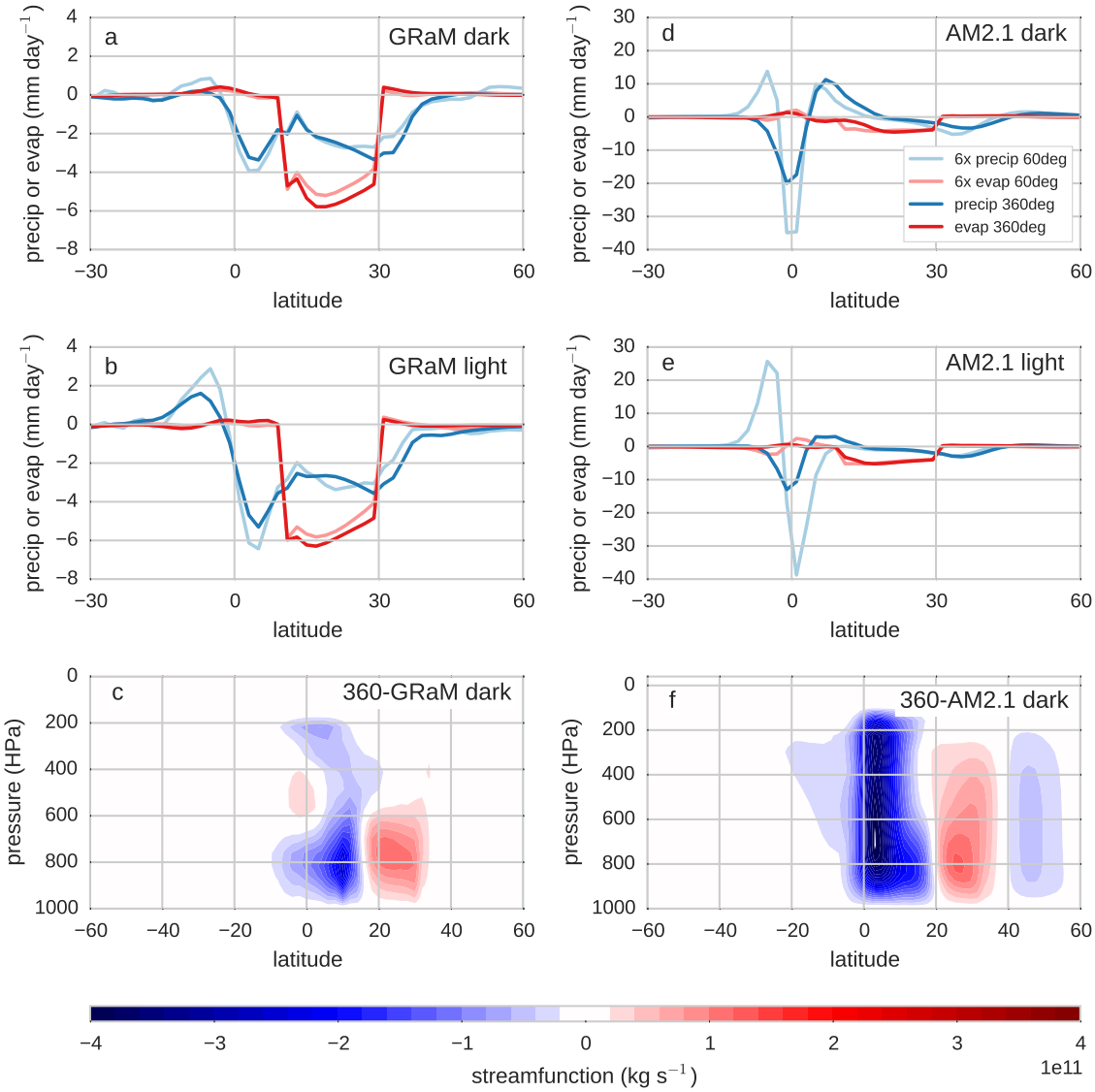

Figure 1. Changes in precipitation, evaporation, and circulation in GRaM and AM2 simulations. Panel a shows the changes in precipitation (blue) and evaporation (red) from simulations with dark continents that are 60° wide (light colors) and 360° wide (dark colors). Panel b shows the equivalent quantities for the same continent but with a brighter land albedo. The changes for the 60° continents have been multiplied by a factor of six for comparison to the 360° simulations. Panel c shows the change in overturning streamfunction for the dark 360° continent GRaM simulation. Panels d-f show equivalent values for the AM2.1 simulations. Changes are relative to each model's aquaplanet simulation.

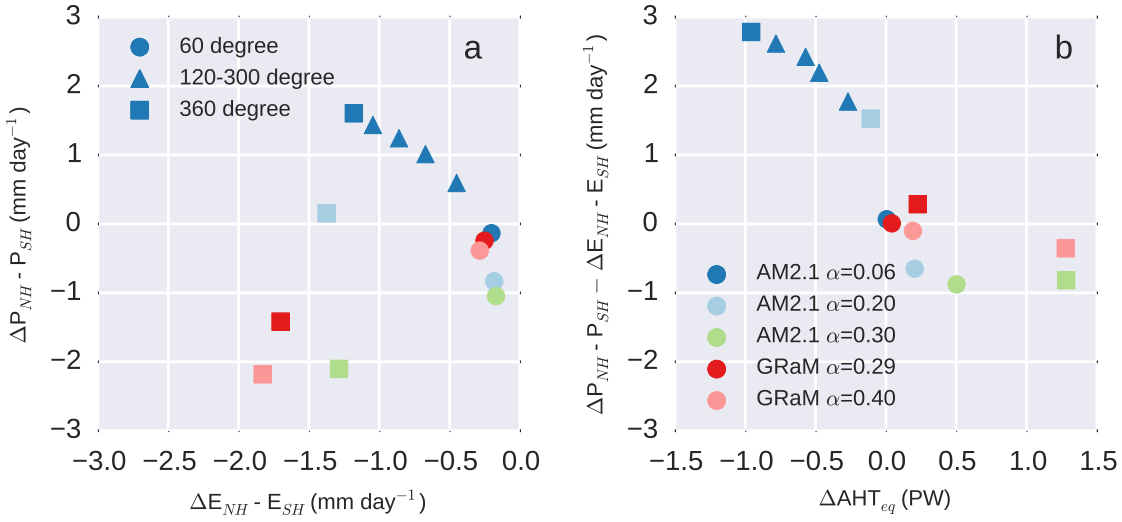

Figure 2. Changes in zonal mean precipitation, evaporation, and cross-equatorial atmosphere heat transport in AM2.1 simulations. Panel a shows the change in NH-SH zonal mean precipitation versus NH-SH zonal mean evaporation. Panel b shows the change in NH-SH zonal average P-E versus the change in cross-equatorial atmospheric energy transport. The NH-SH values are the average precipitation (or evaporation) for the hemisphere. Changes are relative to the aquaplanet simulation. Dark markers indicate the dark continent simulations, while light markers indicate the light continent simulations. Red markers indicate GRaM simulations, while blue and green markers indicate AM2.1 simulations. Circles indicate simulations with 60° wide continents, squares indicate 360° wide simulations, and triangles indicate continents with intermediate width continents.

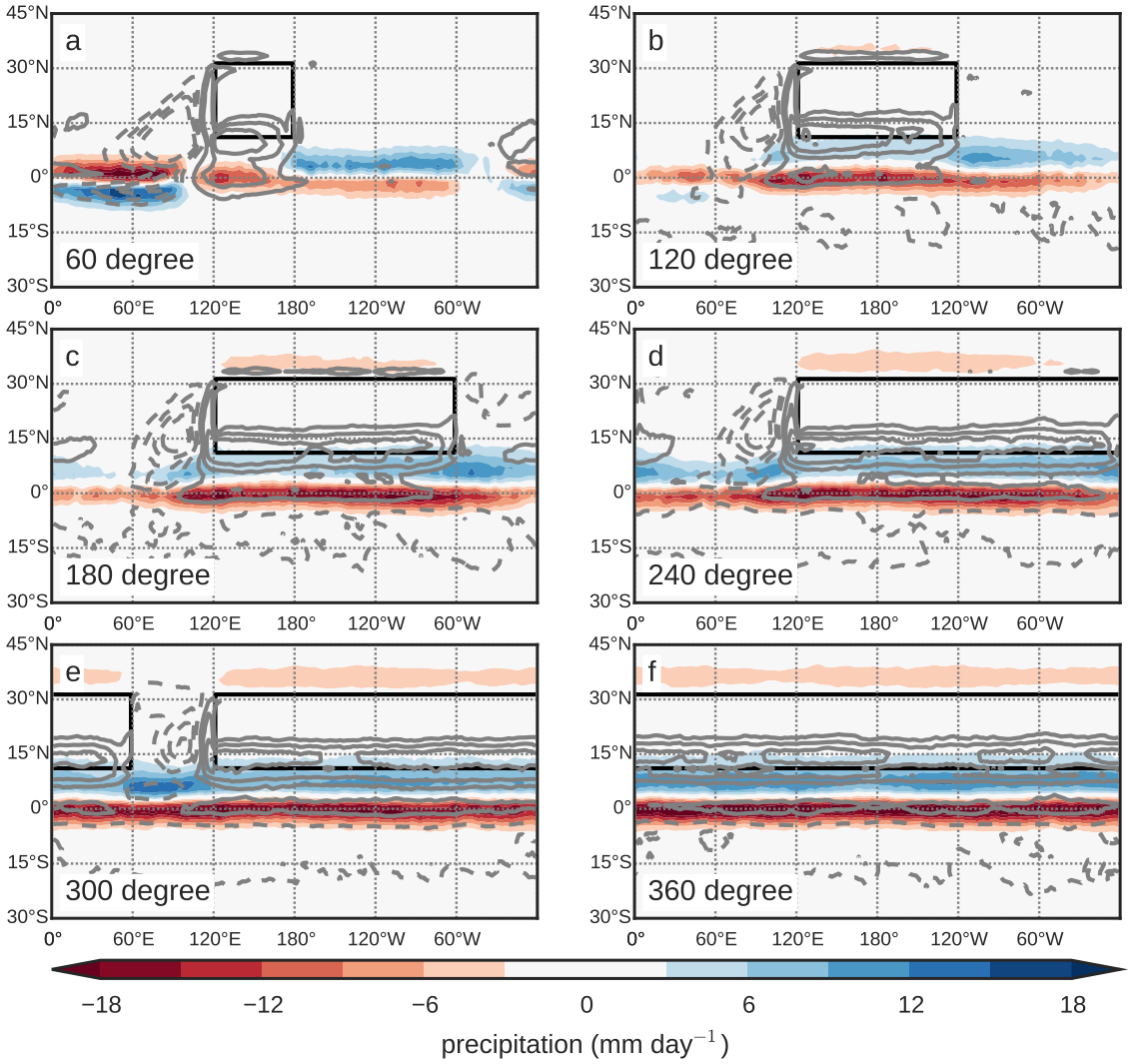

Figure 3. Changes in precipitation (shading) and TOA net radiation (contours) for AM2.1 continent simulations. Changes from the aquaplanet simulation are shown for the 60° (a), 120° (b), 180° (c), 240° (d), 300° (e), and 360° (f) wide continents. Net radiation is defined as positive (solid) where it adds heat to the Earth and negative (dashed) where heat is lost from the Earth. Contours are every 10 W m^{-2}.

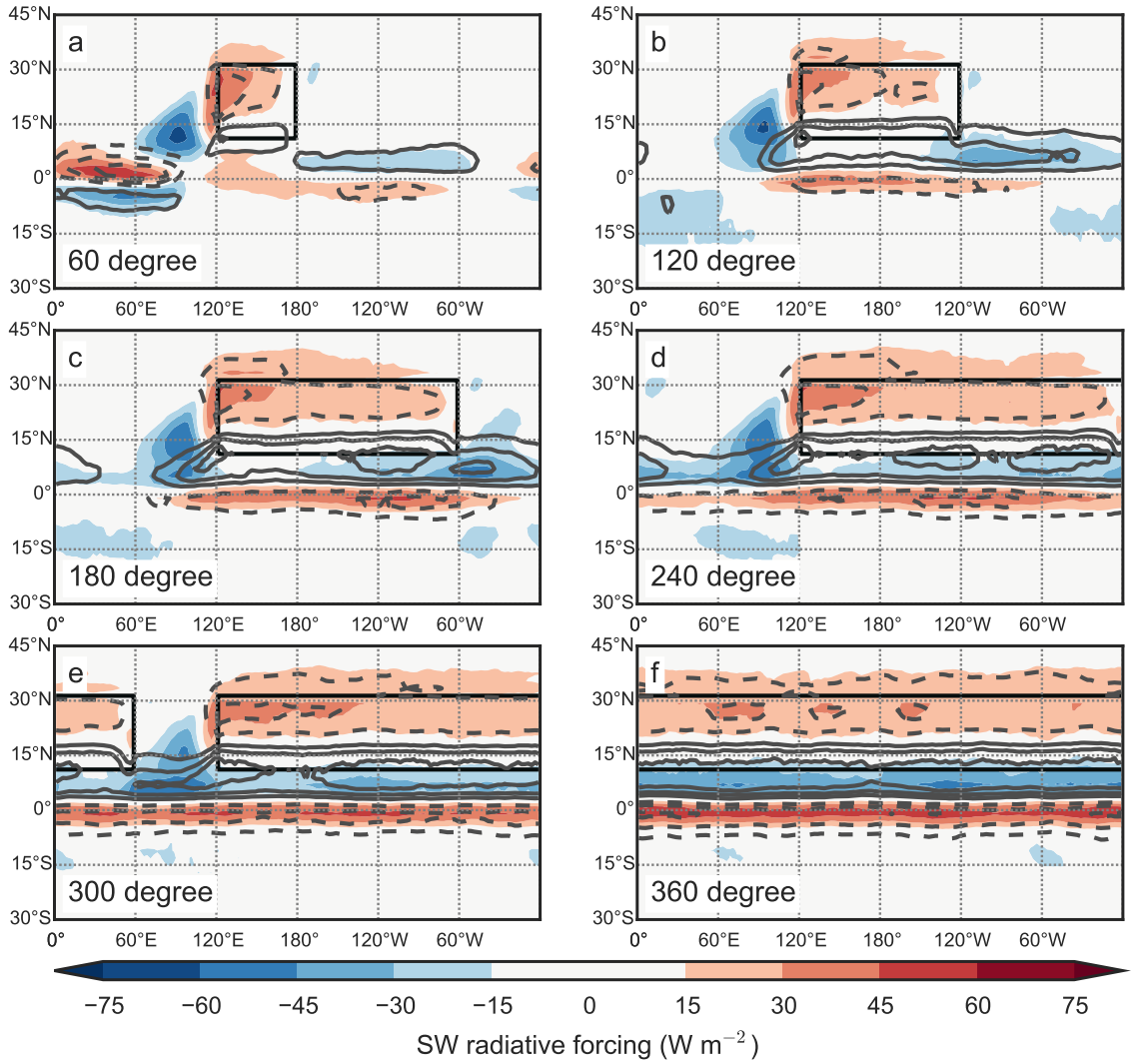

Figure 4. Changes in LW (contours) and SW (shading) for AM2.1 continent simulations. Changes are relative to the aquaplanet and for the same simulations in Figure 3. LW and SW radiation are positive where heat is added to the Earth. Contours and shading are every 15 W m^{-2}. Solid contours are positive while dashed contours are negative.